

## Exciton states and optical spectra in CdSe nanocrystallite quantum dots

Jingbo Li

*National Laboratory for Superlattices and Microstructures, Institute of Semiconductors, Chinese Academy of Sciences, P.O. Box 912, Beijing 100083, People's Republic of China*

Jian-Bai Xia

*China Center of Advanced Sciences and Technology (World Laboratory), P.O. Box 8730, Beijing 100080, People's Republic of China and National Laboratory for Superlattices and Microstructures, Institute of Semiconductors, Chinese Academy of Sciences, P.O. Box 912, Beijing 100083, People's Republic of China*

(Received 22 November 1999)

By using the hole effective-mass Hamiltonian for semiconductors with the wurtzite structure, we have studied the exciton states and optical spectra in CdSe nanocrystallite quantum dots. The intrinsic asymmetry of the hexagonal lattice structure and the effect of spin-orbital coupling (SOC) on the hole states are investigated. It is found that the strong SOC limit is a good approximation for hole states. The selection rules and oscillator strengths for optical transitions between the conduction- and valence-band states are obtained. The Coulomb interaction of exciton states is also taken into account. In order to identify the exciton states, we use the approximation of eliminating the coupling of  $\Gamma_6(X,Y)$  with  $\Gamma_1(Z)$  states. The results are found to account for most of the important features of the experimental photoluminescence excitation spectra of Norris *et al.* However, if the interaction between  $\Gamma_6(X,Y)$  and  $\Gamma_1(Z)$  states is ignored, the optically passive  $P_x$  state cannot become the ground hole state for small CdSe quantum dots of radius less than 30 Å. It is suggested that the intrinsic asymmetry of the hexagonal lattice structure and the coupling of  $\Gamma_6(X,Y)$  with  $\Gamma_1(Z)$  states are important for understanding the “dark exciton” effect.

### I. INTRODUCTION

Recently much attention has been paid to the physics of low-dimensional semiconductor structures. This has been stimulated by the rapid progress in nanometer-scale fabrication technology. Among them, quantum dots (QD's), which are also defined as nanocrystals and microcrystallites, or nanoclusters, are of particular interest. The effect of quantum confinement on the electrons and holes in semiconductor QD's has been studied extensively both theoretically<sup>1–15</sup> and experimentally<sup>16–22</sup> in recent years. The most striking property of semiconductor QD's is the massive change in optical properties as a function of quantum dot size. For example, the band gap in a CdS nanocrystal can be tuned between 4.5 and 2.5 eV as the size is varied from the molecular regime to the macroscopic crystal.

The semiconductor nanocrystal has a prospective application in devices.<sup>20–22</sup> Furthermore, it offers an opportunity to investigate theoretically the inherent physics in such three-dimensionally confined systems. The size-dependent absorption spectra of CdSe or CdS colloids have several well-defined excitonic features that have been convincingly assigned to states derived from a spherical confinement model using the effective-mass approximation.<sup>23,24</sup> However, the observation of the “dark exciton” in recent experiments<sup>25,26</sup> makes it worth endeavoring to study the interesting systems in detail.

Up to now, several different theoretical models have been used in the study of electronic structures of semiconductor QD's. Early on, Efros and Efros<sup>1</sup> described the quantum sphere within the framework of the single-band effective-mass approximation. Taking into account the mixing of hole

states, Xia<sup>2</sup> introduced the Baldereschi-Lipari Hamiltonian<sup>27</sup> to investigate the electronic structure of spherical QD's. Then Murray *et al.*<sup>3</sup> and others<sup>4,5,23,24,28,29</sup> applied the spherical multiband effective-mass theory to study nanocrystallite QD's and found experimental results in good agreement with theoretical predictions. Einevoll and co-workers<sup>6,7</sup> presented an effective bond-orbital model to study the exciton states of semiconductor nanocrystals. Recently, Efros *et al.*<sup>25</sup> developed an eight-band model to calculate the band-edge exciton fine structure in semiconductor QD's. An alternative method is a treatment within the linear combination of atomic orbitals (LCAO) approximation. For example, tight-binding<sup>8–10</sup> and empirical pseudopotential method,<sup>11,12</sup> have been used to calculate the energy states of semiconductor QD's.

The nanocrystallite QD's of II-VI compounds are usually embedded in a large-band-gap matrix, such as glasses, polymers, liquids, rocksalts, or zeolites. For CdSe, CdS, and ZnS nanocrystallites the common lattice structure is hexagonal (wurtzite), as proved by high-resolution transmission electron microscopy TEM and x-ray diffraction.<sup>3</sup> However, the above theoretical work using the effective-mass model was mainly based on a Hamiltonian with zinc-blende structure,<sup>2–4</sup> or treated the crystal-field splitting (due to the hexagonal structure) as a perturbation.<sup>5,7,25</sup> To improve the models further, it is necessary to compare the band structure of zinc-blende semiconductors with that of wurtzite semiconductors.

In Fig. 1 the bulk bands are plotted for zinc-blende and wurtzite crystal structures.<sup>30</sup> The similarity of the two bands is the twofold spin degeneracy at  $k=0$  in the conduction band. Taking into account the spin-orbit interaction, the valence bands are classified according to the total angular momentum  $J$ , which represents the sum of the orbital angular

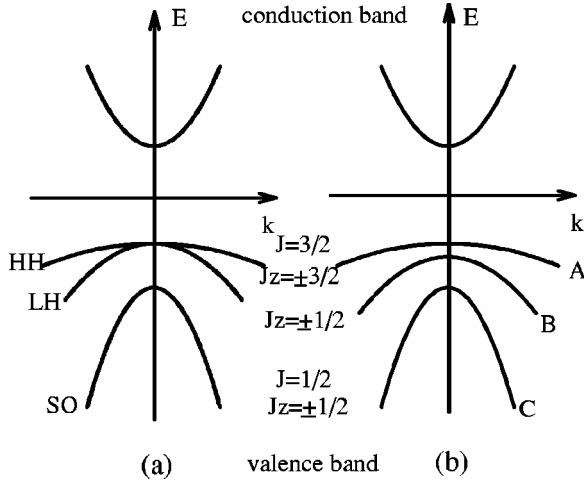


FIG. 1. Scheme of band structure for zinc-blende-type and wurtzite-type semiconductors. Zinc-blende-type band structure is drawn in (a), and wurtzite-type band structure is shown in (b).

momentum and the spin angular momentum. When coupling the orbital momentum  $L$  with the spin momentum  $1/2$ , one may obtain the valence band with a total angular momentum  $J=3/2$  ( $J_z = \pm 3/2, \pm 1/2$ ) or  $J=1/2$  ( $J_z = \pm 1/2$ ). At  $k=0$  (the  $\Gamma$  point of the Brillouin zone) the two bands  $J=3/2$  and  $J=1/2$  are split by the spin-orbit coupling energy  $\Delta_{SO}$ . In Fig. 1(a) the three valence bands of zinc-blende type are defined as the heavy-hole (HH), light-hole (LH), and spin-orbit split-off (SO) bands. The HH and LH subbands are degenerate at the  $\Gamma$  point. In bulk wurtzite semiconductors [Fig. 1(b)], the three valence bands are denoted as the A, B, and C bands.<sup>30</sup> The A band is higher than the B band due to the crystal-field splitting. In our recent work<sup>15</sup> and the present paper, we find that the crystal-field splitting plays an important role in the ground hole state of nanocrystallite QD's.

In this paper we study the exciton states and optical spectra in CdSe QD's. The excitonic binding energies including the Coulomb interaction are calculated. It is found that for the excited hole states, the coupling of  $\Gamma_6(X,Y)$  and  $\Gamma_1(Z)$  states is small and can be neglected. In this approximation our theoretical results are found to account for most of the important features of the experimental optical spectra obtained by Norris *et al.*<sup>23,24</sup> The remainder of the paper is organized as follows. In Sec. II we present the calculation method for the system being considered. Our numerical results and discussion are given in Sec. III. Finally, we draw a brief conclusion in Sec. IV.

## II. CALCULATION METHOD

Using the  $\mathbf{k} \cdot \mathbf{p}$  perturbation method, we have derived the correct effective-mass Hamiltonian for wurtzite semiconductors including the  $p$  linear term.<sup>15,31</sup> The CdSe band structure is calculated by the empirical pseudopotential method, and the effective-mass parameters are determined by fitting the valence-band structure near the top. We do not repeat the details here for the sake of conciseness.

### A. Electronic structure of spherical quantum dot

From the effective-mass parameters for hexagonal semiconductors,<sup>15</sup> we see that the conduction band of the

electron is not isotropic, with different effective masses in the  $z$  and  $x,y$  directions. The effective-mass Hamiltonian of the electron is written as

$$H_e = \frac{1}{2m_x}(p_x^2 + p_y^2) + \frac{1}{2m_z}p_z^2, \quad (1)$$

where  $m_x$  and  $m_z$  are the effective masses in the  $x$  (or  $y$ ) and  $z$  directions, respectively. The Hamiltonian (1) can also be written as

$$H_e = \frac{p^2}{2m_a} - \frac{1}{2m_b} \sqrt{\frac{2}{3}} P_0^{(2)}, \quad (2)$$

with the effective masses

$$\frac{1}{m_a} = \frac{1}{3} \left( \frac{2}{m_x} + \frac{1}{m_z} \right),$$

$$\frac{1}{m_b} = \frac{1}{3} \left( \frac{1}{m_x} - \frac{1}{m_z} \right),$$

where  $P_0^{(2)}$  is the second-order tensor of the momentum operator.

The Hamiltonian (2) couples states with either even angular momentum  $l$  or odd  $l$ ; only the  $z$  component  $m$  is a good quantum number. From Ref. 15 we see that for II-VI compounds the difference between  $m_x$  and  $m_z$  is so small that we can neglect the coupling between different  $l$  states, and consider that  $l$  and  $m$  are good quantum numbers. The eigenenergy of the electron state  $C_{ln}j_l(k_n^l r)$  is

$$E_{l,n} = \frac{\hbar^2}{2m_a} \left( \frac{\alpha_n^l}{R} \right)^2, \quad (3)$$

where  $j_l(x)$  is the spherical Bessel function of order  $l$ ,  $\alpha_n^l = k_n^l R$  is the  $n$ th zero point of  $j_l$ ,  $R$  is the radius of the sphere, and  $C_{l,n}$  is the normalization constant,

$$C_{l,n} = \frac{\sqrt{2}}{R^{3/2}} \frac{1}{j_{l+1}(\alpha_n^l)}.$$

The hole effective-mass Hamiltonian in the zero spin-orbital coupling (SOC) limit is

$$H_h = \frac{1}{2m_0} \begin{vmatrix} P_1 & S & T \\ S^* & P_3 & S \\ T^* & S^* & P_1 \end{vmatrix}, \quad (4)$$

where

$$\begin{aligned}
P_1 &= \gamma_1 p^2 - \sqrt{\frac{2}{3}} \gamma_2 P_0^{(2)}, \\
P_3 &= \gamma'_1 p^2 + 2\sqrt{\frac{2}{3}} \gamma'_2 P_0^{(2)} + 2m_0 \Delta_c, \\
T &= \eta P_{-2}^{(2)} + \delta P_2^{(2)}, \\
T^* &= \eta P_2^{(2)} + \delta P_{-2}^{(2)}, \\
S &= A p_0 P_{-1}^{(1)} + \sqrt{2} \gamma'_3 P_{-1}^{(2)}, \\
S^* &= -A p_0 P_1^{(2)} - \sqrt{2} \gamma'_3 P_1^{(2)},
\end{aligned}$$

and  $P^{(2)}, P^{(1)}$  are the second-order and first-order tensors of the momentum operator, respectively. The effective-mass parameters  $\gamma_1, \gamma_2, \dots$  are related to  $L, M, N, \dots$  as follows:

$$\begin{aligned}
\gamma_1 &= \frac{1}{3}(L+M+N), \quad \gamma_2 = \frac{1}{6}(L+M-2N), \quad \gamma_3 = \frac{1}{6}R, \\
\gamma'_1 &= \frac{1}{3}(T+2S), \quad \gamma'_2 = \frac{1}{6}(T-S), \quad \gamma'_3 = \frac{1}{6}Q, \\
\eta &= \frac{1}{6}(L-M+R), \quad \delta = \frac{1}{6}(L-M-R).
\end{aligned}$$

$L, M, \dots, S, T$  are effective-mass parameters of hexagonal semiconductors taken from Ref. 15.

The basic functions of the valence-band top are  $|11\rangle = (1/\sqrt{2})(X+iY)$ ,  $|10\rangle = Z$ ,  $|1-1\rangle = (1/\sqrt{2})(X-iY)$ , with components of angular momentum 1, 0, and  $-1$ , respectively. Taking  $|11\rangle$ ,  $|10\rangle$ , and  $|1-1\rangle$  as the basic functions, the spin-orbital coupling Hamiltonian is written as<sup>15,32</sup>

$$H_{\text{SO}} = \begin{pmatrix} -\lambda & 0 & 0 & 0 & 0 & 0 \\ 0 & 0 & 0 & \sqrt{2}\lambda & 0 & 0 \\ 0 & 0 & \lambda & 0 & -\sqrt{2}\lambda & 0 \\ 0 & \sqrt{2}\lambda & 0 & \lambda & 0 & 0 \\ 0 & 0 & -\sqrt{2}\lambda & 0 & 0 & 0 \\ 0 & 0 & 0 & 0 & 0 & -\lambda \end{pmatrix}, \quad (5)$$

where the first three basic functions correspond to spin-up states, the second three basic functions correspond to spin-down states,

$$\lambda = \frac{\hbar^3}{4m_0^2 c^2} \left\langle X \left| \frac{\partial V}{\partial x} \frac{\partial}{\partial y} \right| Y \right\rangle = \frac{\Delta_{\text{SO}}}{3}, \quad (6)$$

and  $\Delta_{\text{SO}}$  is the spin-orbital splitting energy.

The eigenenergies and corresponding eigenstates in quantum spheres are calculated as in Refs. 32 and 15. The wave functions are expanded with spherical Bessel functions and spherical harmonic functions for the zero SOC case,

$$\Psi_h = \sum_{l,n} \begin{pmatrix} a_{l,n} C_{l,n} j_l(k_n^l r) Y_{l,m-1}(\theta, \phi) \\ b_{l,n} C_{l,n} j_l(k_n^l r) Y_{l,m}(\theta, \phi) \\ d_{l,n} C_{l,n} j_l(k_n^l r) Y_{l,m+1}(\theta, \phi) \end{pmatrix}. \quad (7)$$

Because of the hexagonal symmetry only the  $z$  component of the angular momentum  $J_z$  is a good quantum number. The linear terms in the Hamiltonian (4) couple the states of even angular momentum  $l$  and odd  $l$ , and the summation over  $l$  in the expansion of wave function (7) includes both even and odd  $l$ , different from the case of zinc-blende semiconductors. In that case,<sup>32</sup> the summation over  $l$  includes either even  $l$  or odd  $l$  due to the second-order tensor operators.

In the case of finite SOC, we start from the hole Hamiltonian (4) for both states (spin up and spin down), to which we add the SOC Hamiltonian (5), and keep the  $z$  component of the total angular momentum as a constant. For example, if we take  $J_z = 0$  in Eq. (7) for the first three basic functions, then we take  $J_z = 1$  in Eq. (7) for the second three basic functions, in order that the  $z$  component of the total angular momentum be  $1/2$ .

In order to study the SOC effect, we calculate the hole subband structure from the finite SOC to the strong SOC limit ( $\lambda \rightarrow \infty$ ). The corresponding hole Hamiltonians are  $6 \times 6$  and  $4 \times 4$  dimensional matrices, respectively. As a result, the hole effective-mass Hamiltonian with wurtzite structure in the strong SOC limit is

$$H_h = \frac{1}{2m_0} \begin{pmatrix} P_1 & -\sqrt{\frac{2}{3}}S & \frac{1}{\sqrt{3}}T & 0 \\ -\sqrt{\frac{2}{3}}S^* & \frac{1}{3}P_1 + \frac{2}{3}P_3 & 0 & \frac{1}{\sqrt{3}}T \\ \frac{1}{\sqrt{3}}T^* & 0 & \frac{1}{3}P_1 + \frac{2}{3}P_3 & \sqrt{\frac{2}{3}}S \\ 0 & \frac{1}{\sqrt{3}}T^* & \sqrt{\frac{2}{3}}S^* & P_1 \end{pmatrix}. \quad (8)$$

The basic functions of Hamiltonian (8) in the valence-band top are  $|\frac{3}{2}, \frac{3}{2}\rangle$ ,  $|\frac{3}{2}, \frac{1}{2}\rangle$ ,  $|\frac{3}{2}, -\frac{1}{2}\rangle$ , and  $|\frac{3}{2}, -\frac{3}{2}\rangle$ .

## B. Oscillator strength of optical transition

First, we ignore the exciton effect and calculate the oscillator strength of the optical transition between the conduction- and valence-band states. The optical-transition matrix element can be calculated by

$$\begin{aligned}
\langle \Phi_e | \mathbf{p} | \Phi_h \rangle &= \int r^2 dr f_e(r) f_h(r) \langle l_e m_e | l_h m_h \rangle \langle c | \mathbf{p} | v \rangle \\
&= \sum_L \int r^2 dr f_e(r) f_h(r) \sum_{M_1} \langle c | \mathbf{p} | v \rangle \\
&= I_{eh} \mathbf{p}_{cv} \delta_{l_e l_h} \delta_{m_e m_h},
\end{aligned}$$

where  $f_e(r)$  [ $f_h(r)$ ] is the electron (hole) radial wave function,  $|lm\rangle$  is the angular wave function.  $|c\rangle$  and  $|v\rangle$  are the Bloch wave functions at the conduction-band bottom and valence-band top.  $I_{eh}$  is the overlap integral for the envelope functions of electrons and holes. Then the oscillator strength of the optical transition is given by

$$K = |I_{eh}|^2. \quad (9)$$

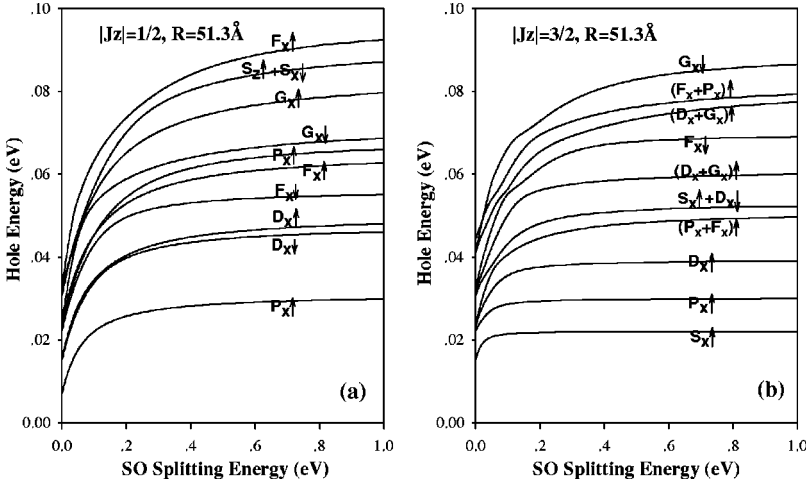


FIG. 2. Hole energies for several states as functions of the spin-orbital splitting energy for a fixed dot radius  $R = 51.8 \text{ \AA}$ . In (a)  $|J_z| = 1/2$  and in (b)  $|J_z| = 3/2$ .

### C. Exciton states

If we take the electronic Bohr radius  $a_e^* = \hbar^2 \epsilon_r / m_e^* e^2$  and Rydberg  $R_e^* = m_e^* e^4 / 2 \hbar^2 \epsilon_r^2$  ( $m_e^*$  is the effective mass of the electron in units of the free electron mass  $m_0$ , and  $\epsilon_r$  is the dielectric constant of the material) as the units of length and energy, the exciton Hamiltonian in a quantum sphere can be written as

$$H = H_0 + V_{e-h}, \quad (10)$$

$$H_0 = H_e + H_h + H_{SO} + V_e(r) + V_h(r), \quad (11)$$

$$V_{e-h} = -\frac{2}{r_{eh}}, \quad (12)$$

where  $e(h)$  refers to electron (hole), and  $V_e$  ( $V_h$ ) is the confined potential of the electron (hole).  $V_{e-h}$  is the Coulomb interaction term between the electron and hole.

The exciton wave function can be expanded in terms of electron and hole wave functions as

$$\Psi_{ex} = \sum_{i,j} c_{ij} \Psi_{ei}(\mathbf{r}_e) \Psi_{hj}(\mathbf{r}_h), \quad (13)$$

where  $\Psi_{ei}(\mathbf{r}_{ei})$  and  $\Psi_{hj}(\mathbf{r}_{hj})$  are the wave functions of electronic and hole eigenstates, respectively. The matrix element of the Coulomb interaction can be calculated by using

$$\frac{1}{r_{eh}} = \sum_{k=0}^{\infty} \frac{r_{<}^k}{r_{>}^{k+1}} P_k(\cos \theta_{eh}), \quad (14)$$

$$P_k(\cos \theta_{eh}) = \frac{4\pi}{2k+1} \sum_{m=-k}^k Y_{km}^*(\theta_e, \varphi_e) Y_{km}(\theta_h, \varphi_h), \quad (15)$$

where  $P_k$  are the Legendre polynomials,  $\theta_{eh}$  is the angle between the position vectors of electron ( $\mathbf{r}_e$ ) and hole ( $\mathbf{r}_h$ ),  $r_{<} \equiv \min(r_e, r_h)$ , and  $r_{>} \equiv \max(r_e, r_h)$ .<sup>33</sup>

The exciton energy can be obtained from the secular equation

$$|(E_{n_e, l_e} + E_{m_h, l_h} - E) \delta_{ij} + V_{ij}| = 0. \quad (16)$$

The matrix element of the Coulomb interaction  $V_{ij}$  is given by

$$\left\langle \frac{1}{r_{eh}} \right\rangle = \sum_{l,k} R^k \frac{4\pi}{2k+1} \sum_{m=-k}^k (-1)^m \langle Y_{l'm_e} | Y_{k-m} | Y_{l_e m_e} \rangle \langle Y_{l'_h m'_h} | Y_{km} | Y_{l_h m_h} \rangle, \quad (17)$$

where

$$R^k = \sum_l \int_0^\infty \int_0^\infty R_e(n_e, l_e, m_e) R_e(n'_e, l'_e, m'_e) \times R_h(n_h, l_h, m_h) R_e(n'_h, l'_h, m'_h) \frac{r_{<}^k}{r_{>}^{k+1}} r_e^2 r_h^2 dr_e dr_h, \quad (18)$$

$$\begin{aligned} \langle Y_{l'm'} | Y_{km} | Y_{lm} \rangle &= \int_0^{2\pi} \int_0^\pi Y_{l'm'}(\theta, \varphi) \\ &\times Y_{km}(\theta, \varphi) Y_{lm}(\theta, \varphi) \sin(\theta) d\theta d\varphi \\ &= \left( \frac{(2l'+1)(2l+1)(2k+1)}{4\pi} \right)^{1/2} \\ &\times \begin{pmatrix} k & l_h & l'_h \\ 0 & 0 & 0 \end{pmatrix} \\ &\times \begin{pmatrix} k & l_h & l'_h \\ m & m_h & m'_h \end{pmatrix}. \end{aligned} \quad (19)$$

### III. NUMERICAL RESULTS AND DISCUSSION

In this section we use CdSe QD's as a model system to make a numerical computation. The parameters concerned are taken from Ref. 30: the hexagonal lattice constants  $a = 4.30 \text{ \AA}$ ,  $c = 7.02 \text{ \AA}$ , the spin-orbit splitting  $\Delta_{SO} = 0.42 \text{ eV}$ , and the crystal-field splitting  $\Delta_c = 40 \text{ meV}$ . CdSe QD's can be embedded in different types of material. The values of the electron band offset  $V_e$  and hole band offset  $V_h$  for these structures are generally unknown. In this paper, the hole calculations assume an infinite potential boundary condition, while a finite barrier for electrons ( $V_e$ ) is used for comparing with experimental data. The best fit requires that  $V_e = 9.0 \text{ eV}$ . It is obvious that this parameter is not physically

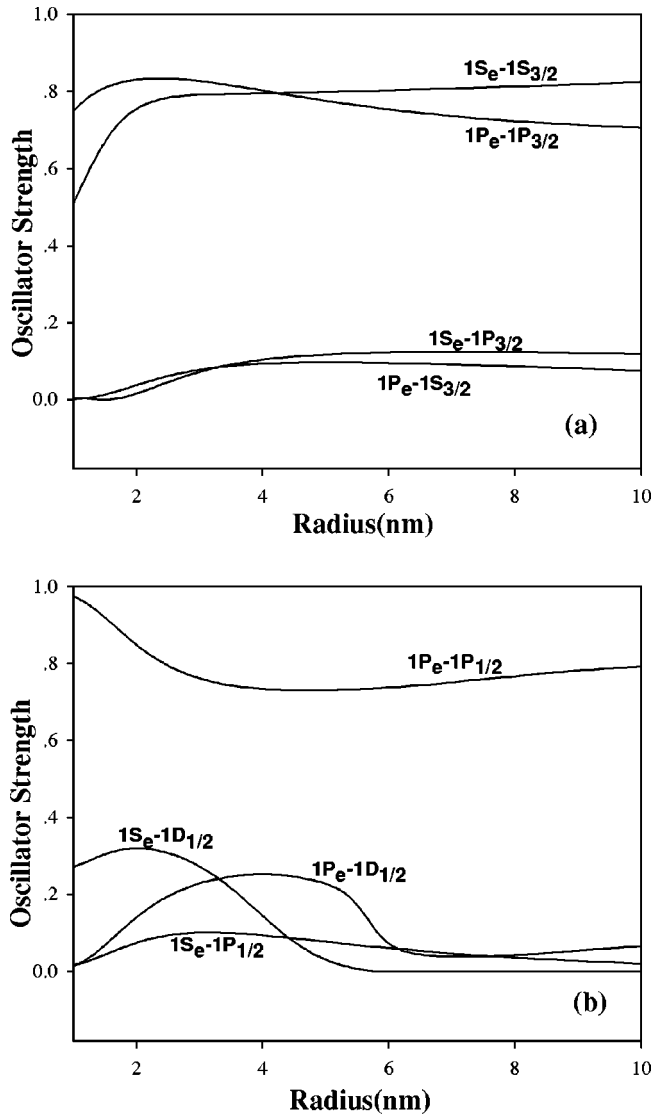


FIG. 3. Oscillator strength as a function of the dot radius  $R$  in the case of (a)  $|J_z|=1/2$  and (b)  $|J_z|=3/2$ .

meaningful, and in practice  $V_e$  is used as a fitting parameter.

Figure 2 exhibits the hole energy spectra as functions of spin-orbit splitting energy  $\Delta_{SO}$ . There are many degenerate states at  $\Delta_{SO}=0$ , e.g.,  $D_x\uparrow$  and  $D_x\downarrow$  in Fig. 2(a), and they would be split at finite SO splitting energy due to the spin-orbit coupling. In both Figs. 2(a) and 2(b) the excited hole states are observed to cross when the SO splitting energy is small. The crossings of hole states are very sensitive to the SO splitting energy in the interval  $0 < \Delta_{SO} < 0.3$  eV. It is shown that the strong SOC limit (i.e.,  $\Delta_{SO} \rightarrow \infty$ ) is a good approximation for CdSe (with  $\Delta_{SO}=0.42$  eV) QD's for the ground hole states ( $P_x$  with  $|J_z|=1/2$ , and  $S_x$  with  $|J_z|=3/2$ ). However, for the high excited hole states with  $|J_z|=1/2$ , for example, the  $F_x\uparrow$  state in Fig. 2(a), this approximation would not be appropriate because these states are mainly affected by the split-off band [ $C$  band in Fig. 1(b)]. Figure 2 only plots the case for a fixed dot radius  $R=51.3$  Å, but similar results would be given for other radii.

In Fig. 3 we plot the oscillator strength of the optical transitions between the electron and hole states as functions of the dot radius. The strongest transitions are  $1S_e-1S_{3/2}$ ,

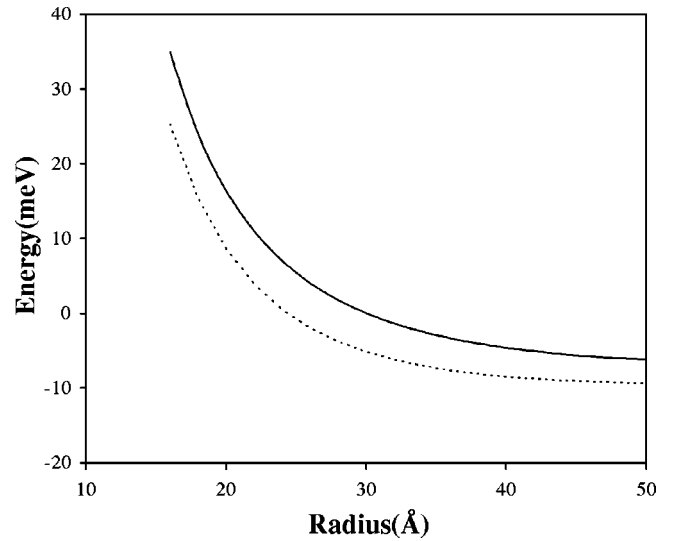


FIG. 4. Energy differences of  $S_x(|J_z|=3/2)$  and  $P_x(|J_z|=1/2)$  states as functions of the dot radius. The result without exciton effect is plotted as the solid curve, while the result with exciton effect is shown as the dotted curve.

$1P_e-1P_{3/2}$ , and  $1P_e-1P_{1/2}$ . Since it is hard to identify high excited hole states such as the  $2S_{3/2}$  state, we show only some transition oscillator strengths of lower states. It is easily found that the selection rule of optical transitions in a wurtzite-type semiconductor nanocrystal is  $\Delta L=0, \pm 1, \pm 2$ . The transitions do not follow the selection rule  $\Delta L=0, \pm 2$  strictly any more.<sup>2</sup> This is because the linear terms in the Hamiltonian (4) couple states of even angular momentum  $l$  and odd  $l$ . However, transitions between  $s$ -type and  $p$ -type wave functions such as  $1S_e-1P_{3/2}$  and  $1P_e-1S_{3/2}$  in Fig. 3(a), and  $1S_e-1P_{1/2}$  in Fig. 3(b), exhibit quite small oscillator strengths.

The energy difference of  $S_x$  and  $P_x$  states as a function of the dot radius  $R$  is shown in Fig. 4. The solid curve is plotted without taking into account the exciton effect (this is also depicted in Ref. 15), while the dotted curve shows the case with the exciton effect. Comparing the two curves, we can find that the result with the exciton effect is more consistent with the experimental results of resonant Stokes shift reported by Efros *et al.*<sup>25</sup>

Now we discuss the relationship between the exciton states and the optical spectra in CdSe QD's. Norris *et al.*<sup>23,24</sup> investigated the photoluminescence excitation (PLE) spectroscopy to avoid the competition between bleach features and induced absorptions that complicates the analysis. As for our theoretical model presented in this paper, due to hole state mixing, it is difficult to assign the high-hole states in the strong confinement regime.<sup>15</sup> But we found that for the excited hole states the coupling of  $\Gamma_6(X,Y)$  with  $\Gamma_1(Z)$  states is small and can be neglected. In this approximation we calculated the spectra of CdSe QD's.

Our results for the size-dependent spectra of CdSe QD's in the strong confinement regime are shown in Fig. 5 and Fig. 6. The  $x$  axis of the two figures is the energy of the ground exciton state (i.e., the first excited state), because the energy is more easily and precisely measured experimentally than the dot size due to sample inhomogeneities. Using the dot radius as the  $x$  axis will induce significant error in the

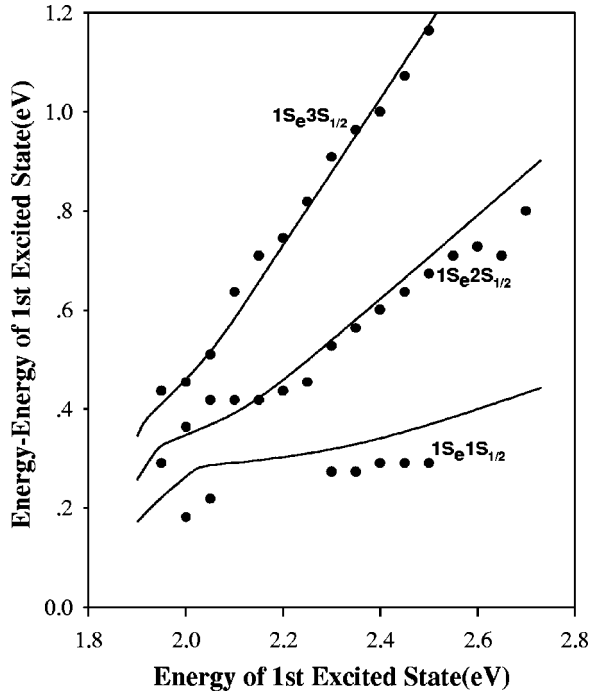


FIG. 5. Comparison with experiments for excited exciton states. The excited-state energies are shown as functions of the energy of the first excited state (i.e., the ground-state exciton energy). Solid curves correspond to  $1S_e1S_{1/2}$ ,  $1S_e2S_{1/2}$ , and  $1S_e3S_{1/2}$  states. Experimental results of Norris *et al.* (Ref. 14) on CdSe quantum dots are marked as circles.

size measurement; therefore, the energy of the first excited state can describe the probed dots better. The energy of the  $y$  axis is relative to the ground exciton state. As mentioned above, when the interaction between  $\Gamma_6(X,Y)$  and  $\Gamma_1(Z)$  states is ignored, the ground exciton state is  $1S_e1S_{3/2}$  in our calculation. Figure 5 shows  $1S_e1S_{1/2}$ ,  $1S_e2S_{1/2}$ , and  $1S_e3S_{1/2}$  exciton energy spectra by the solid curves. The data points are experimental data from Ref. 24. The figure indicates that the theory is in agreement with the experimental results. Figure 6 depicts the spectra of the  $1S_e2S_{3/2}$  and  $1P_e1P_{3/2}$  states. From Fig. 3 we see that the  $1S_e1S_{3/2}$  and  $1P_e1P_{3/2}$  should be the two strongest transitions, which is consistent with experimental observations.<sup>24</sup> In Fig. 6 the dotted curve represents the relative exciton energy of the  $1P_e1P_{1/2}$  state and is compared with that of the  $1P_e1P_{1/2}$  state.

The assumption of  $S=0$  in Hamiltonian (4), i.e., elimination of the coupling of  $\Gamma_6(X,Y)$  with  $\Gamma_1(Z)$  states, has a great effect on the  $1P_{1/2}$  hole state, and it would not be the ground hole state for small dots whose radius is smaller than  $30 \text{ \AA}$ .<sup>15</sup> Taking the coupling [ $\Gamma_6(X,Y)$  with  $\Gamma_1(Z)$  states] into consideration, the actual energy of the  $1P_e1P_{1/2}$  state would be smaller than that of  $1P_e1P_{3/2}$  in the strong confinement regime. Consequently, we think that the highest exciton state in Fig. 6 should not be assigned to  $1P_e1P_{1/2}$ , but to  $1P_e1F_{1/2}$ . Additionally, the above discussion also in-

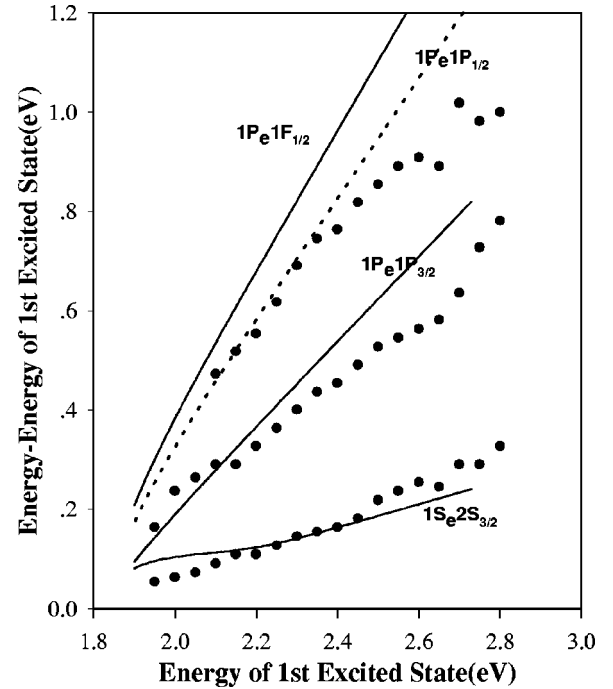


FIG. 6. Same as Fig. 5, but the solid curves correspond to  $1S_e2S_{3/2}$ ,  $1P_e1P_{3/2}$ , and  $1P_e1F_{1/2}$  states. The dotted curve corresponds to the  $1P_e1P_{1/2}$  state.

dicates that the coupling of  $\Gamma_6(X,Y)$  with  $\Gamma_1(Z)$  states in Hamiltonian (4) is important for the “dark exciton” theory.

#### IV. CONCLUSION

In this paper, we have studied the exciton states of CdSe nanocrystallite quantum dots, including the Coulomb interaction between electron and hole. It is found that the strong SOC limit is a good approximation for the hole state. The linear terms in the hole Hamiltonian make it possible for transitions to occur between states with angular momentum  $l$  and  $l \pm 1$ . Taking into account the exciton effect, our numerical result is in agreement with the experimental results for the resonant Stokes shift.<sup>25</sup> In order to identify the exciton states, we use the approximation of eliminating the coupling of  $\Gamma_6(X,Y)$  and  $\Gamma_1(Z)$  states. The results are found to account for most of the important features of the experimental optical spectra of Norris *et al.* However, if the interaction between  $\Gamma_6(X,Y)$  and  $\Gamma_1(Z)$  states is ignored, the optically passive  $P_x$  state cannot become the ground state for small CdSe quantum dots of radius less than  $30 \text{ \AA}$ . Only if the inherent asymmetry of the hexagonal lattice structure and the coupling of  $\Gamma_6(X,Y)$  with  $\Gamma_1(Z)$  states are taken into account for calculating the electronic structure of CdSe nanocrystals, can the “dark exciton” be well explained.

#### ACKNOWLEDGMENTS

This work was supported by the Chinese National Natural Science Foundation. J.L. thanks Professor Desheng Jiang for helpful discussions.

- <sup>1</sup> A.I.L. Efros and A.L. Efros, *Fiz. Tekh. Poluprovodn.* **16**, 1209 (1982) [*Sov. Phys. Semicond.* **16**, 772 (1982)].
- <sup>2</sup> J.B. Xia, *Phys. Rev. B* **40**, 8500 (1989).
- <sup>3</sup> C.B. Murray, D.J. Norris, and M.G. Bawendi, *J. Am. Chem. Soc.* **115**, 8706 (1993).
- <sup>4</sup> A.I. Ekimov, F. Hache, M.C. Schanne-Klein, D. Ricard, C. Flytzanis, I.A. Kudryavtsev, T.V. Yazeva, A.V. Rodina, and A.I.L. Efros, *J. Opt. Soc. Am. B* **10**, 100 (1993).
- <sup>5</sup> A.I.L. Efros, *Phys. Rev. B* **46**, 7448 (1992).
- <sup>6</sup> G.T. Einevoll, *Phys. Rev. B* **45**, 3410 (1992).
- <sup>7</sup> U.E.H. Laheld and G.T. Einevoll, *Phys. Rev. B* **55**, 5184 (1997).
- <sup>8</sup> Y. Wang and N. Herron, *Phys. Rev. B* **42**, 7253 (1990).
- <sup>9</sup> P.E. Lippens and M. Lannoo, *Phys. Rev. B* **41**, 6079 (1990).
- <sup>10</sup> H.H. von Grunberg, *Phys. Rev. B* **55**, 2293 (1997).
- <sup>11</sup> M.V.R. Krishna and R.A. Friesner, *Phys. Rev. Lett.* **67**, 629 (1991).
- <sup>12</sup> L.W. Wang and A. Zunger, *Phys. Rev. B* **53**, 9579 (1996).
- <sup>13</sup> K. Chang and J.B. Xia, *J. Appl. Phys.* **84**, 1454 (1998).
- <sup>14</sup> K. Chang and J.B. Xia, *Phys. Rev. B* **57**, 9780 (1998).
- <sup>15</sup> J.B. Xia and J.B. Li, *Phys. Rev. B* **60**, 11 540 (1999).
- <sup>16</sup> L.E. Brus, *J. Chem. Phys.* **80**, 4403 (1984).
- <sup>17</sup> R. Rossetti, R. Hull, J.M. Gibson, and L.E. Brus, *J. Chem. Phys.* **82**, 552 (1985).
- <sup>18</sup> F.V. Mikulec, B.O. Dabbousi, J. Rodriguez-Viejo, J. R. Heine, H. Mattoussi, K.F. Jensen, and M.G. Bawendi, in *Advances in Microcrystalline and Nanocrystalline Semiconductors—1996*, edited by R.W. Collins, P.M. Fauchet, I. Shimizu, J.-C. Vial, T. Shimada, and P.A. Alivisatos, MRS Symposia Proceedings No. 452 (Materials Research Society, Pittsburgh, 1997), p. 359.
- <sup>19</sup> S.A. Empedocles, D.J. Norris, and M.G. Bawendi, in *Advances in Microcrystalline and Nanocrystalline Semiconductors—1996*, (Ref. 18), p. 335.
- <sup>20</sup> A.P. Alivisatos, *Science* **271**, 933 (1996).
- <sup>21</sup> D.L. Klein, R. Roth, A.K.L. Lim, A.P. Alivisatos, and P.L. McEuen, *Nature (London)* **389**, 699 (1997).
- <sup>22</sup> S.A. Empedocles and M.G. Bawendi, *Science* **278**, 2114 (1997).
- <sup>23</sup> D.J. Norris, A. Sacra, C.B. Murray, and M.G. Bawendi, *Phys. Rev. Lett.* **72**, 2612 (1994).
- <sup>24</sup> D.J. Norris and M.G. Bawendi, *Phys. Rev. B* **53**, 16 338 (1996).
- <sup>25</sup> A.I.L. Efros, M. Rosen, M. Kuno, M. Nirmal, D.J. Norris, and M.G. Bawendi, *Phys. Rev. B* **54**, 4843 (1996).
- <sup>26</sup> M. Nirmal, D.J. Norris, M. Kuno, M.G. Bawendi, A.I.L. Efros, and M. Rosen, *Phys. Rev. Lett.* **75**, 3728 (1995).
- <sup>27</sup> A. Baldereschi and N.O. Lipari, *Phys. Rev. B* **3**, 439 (1971); **8**, 2697 (1973).
- <sup>28</sup> D.J. Norris, A.I.L. Efros, M. Rosen, and M.G. Bawendi, *Phys. Rev. B* **53**, 16 347 (1996).
- <sup>29</sup> S.A. Empedocles, D.J. Norris, and M.G. Bawendi, *Phys. Rev. Lett.* **77**, 3873 (1996).
- <sup>30</sup> *Numerical Data and Functional Relationships in Science and Technology*, edited by O. Madelung, M. Schultz, and H. Weiss, Landolt-Börnstein, New Series, Group III, Vol. 17, Pt. b (Springer, Berlin, 1982).
- <sup>31</sup> J.B. Xia, K.W. Cheah, X.L. Wang, D.Z. Sun, and M.Y. Kong, *Phys. Rev. B* **59**, 10 119 (1999).
- <sup>32</sup> J.B. Xia, *J. Lumin.* **70**, 120 (1996).
- <sup>33</sup> A.R. Edmonds, *Angular Momentum in Quantum Mechanics* (Princeton University Press, Princeton, NJ, 1957).